Experimental Neurology 291 (2017) 106–119

Contents lists available at ScienceDirect

Experimental Neurology

journal homepage: www.elsevier.com/locate/yexnr

Research Paper

Progressive leukoencephalopathy impairs neurobehavioral development in sialin-deficient mice

Stijn Stroobants [a,*,1], Nathalie G.G. Van Acker [c,1], Frans W. Verheijen [b,1], Ilse Goris [d], Guy F.T. Daneels [d], Rachel Schot [b], Elly Verbeek [b,2], Michiel W.M. Knaapen [c], An De Bondt [d], Hinrich W. Göhlmann [d], Marion L.A. Crauwels [e], Grazia M.S. Mancini [b], Luc J. Andries [c], Dieder W.E. Moechars [d], Rudi D'Hooge [a]

[a] Laboratory of Biological Psychology, KU Leuven, Belgium
[b] Dept. Clinical Genetics, Erasmus University Medical Center, Rotterdam, The Netherlands
[c] HistoGeneX, Antwerp, Belgium
[d] Research and Early Development Europe, J&J Pharmaceutical Research & Development, Beerse, Belgium
[e] Dept. Biology, KU Leuven, Belgium

ARTICLE INFO

Article history:
Received 8 April 2016
Received in revised form 25 January 2017
Accepted 7 February 2017
Available online 09 February 2017

Keywords:
Sialic acid storage disease
Mouse model
Sialin
Myelination
Oligodendrocyte lineage
Development
Behavior

ABSTRACT

Slc17a5$^{-/-}$ mice represent an animal model for the infantile form of sialic acid storage disease (SASD). We analyzed genetic and histological time-course expression of myelin and oligodendrocyte (OL) lineage markers in different parts of the CNS, and related this to postnatal neurobehavioral development in these mice. Sialin-deficient mice display a distinct spatiotemporal pattern of sialic acid storage, CNS hypomyelination and leukoencephalopathy. Whereas few genes are differentially expressed in the perinatal stage (p0), microarray analysis revealed increased differential gene expression in later postnatal stages (p10–p18). This included progressive upregulation of neuroinflammatory genes, as well as continuous down-regulation of genes that encode myelin constituents and typical OL lineage markers. Age-related histopathological analysis indicates that initial myelination occurs normally in hindbrain regions, but progression to more frontal areas is affected in *Slc17a5*$^{-/-}$ mice. This course of progressive leukoencephalopathy and CNS hypomyelination delays neurobehavioral development in sialin-deficient mice. *Slc17a5*$^{-/-}$ mice successfully achieve early neurobehavioral milestones, but exhibit progressive delay of later-stage sensory and motor milestones. The present findings may contribute to further understanding of the processes of CNS myelination as well as help to develop therapeutic strategies for SASD and other myelination disorders.

1. Introduction

Sialic acid storage disease (SASD) is an autosomal recessive lysosomal storage disorder caused by deficiency of the lysosomal membrane transporter sialin, and ensuing intralysosomal accumulation of free sialic acid and other acidic monosaccharides. Sialin is encoded by the *SLC17A5* gene, mutations of which give rise to SASD (Mancini et al., 1989; Mancini et al., 1991; Havelaar et al., 1998; Verheijen et al., 1999). Salla disease (OMIM #604369) and infantile sialic acid storage disease (ISSD; OMIM #269920) represent 2 major clinical phenotypes

Abbreviations: (4V), 4th ventricle; (AR), air righting; (aca), anterior commissure; (alv), alveus of the hippocampus; (av), arbor vitae cerebellum; (AS), auditory startle; (CA), cliff aversion; (CNS), central nervous system; (CC), corpus callosum; (cg), cingulum; (Cnp1), cyclic nucleotide phosphodiesterase 1; (dc), dorsal cochlear nucleus; (dg), dentate gyrus; (ET), ear twitch; (ec), external capsule; (fi), fimbria; (fl), flocculus; (FG), forelimb grasping; (Galc), galactosylceramidase; (HPS), hematoxylin phloxin saffrane; (icp), inferior cerebellar peduncle; (ISSD), infantile sialic acid storage disorder; (LD), locomotion development; (LAMP-1), lysosomal associated membrane protein, isoform 1; (Mpeg1), macrophage expressed gene 1; (mt), mammilothalamic tract; (MEF), mouse embryonic fibroblast; (MBP), myelin basic protein; (Mag), myelin-associated glycoprotein; (Mopb), myelin-associated oligodendrocytic basic protein; (Myrf), myelin regulatory factor; (NG), negative geotaxis; (Cspg4), NG2 chondroitin sulphate proteoglycan; (OL), oligodendrocyte; (OP), oligodendrocyte progenitors; (Omg), oligodendrocyte-myelin glycoprotein; (PNS), peripheral nervous system; (Pdgfra), platelet-derived growth factor-α; (PSA-NCAM), polysialylated neural cell adhesion molecule; (Plp1), proteolipid protein 1; (py), pyramidal tract; (RLV), rat liver lysosomal vesicles; (SASD), sialic acid storage disease; (SAM), significance analysis of microarray; (sp5), spinal trigeminal tract; (SVZ), subventricular zone; (SR), surface righting; (vcp), ventral cerebellar peduncle.

* Corresponding author at: Laboratory of Biological Psychology, KU Leuven, Tiensestraat 102, 3000 Leuven, Belgium.
E-mail address: stijn.stroobants@ppw.kuleuven.be (S. Stroobants).
[1] These authors contributed equally to this manuscript.
[2] Deceased.

http://dx.doi.org/10.1016/j.expneurol.2017.02.009

of SASD at either end of the disease spectrum. Children suffering from ISSD present with severe neurodevelopmental defects that rapidly deteriorate, leading to early death. Salla disease does involve psychomotor and cognitive disability, but patients experience a slower deterioration than ISSD patients and survive into adulthood (Haataja et al., 1994).

Myelination defects occur in clinical SASD as well as in mice with sialin deficiency (Prolo et al., 2009), but little is known about their progression and pathological concomitants. SASD leads to progressive cerebellar atrophy as well as decreased cerebral white matter volume, which have been suggested to be caused by hypomyelination (i.e., insufficient myelin deposition and/or maturation), rather than myelin breakdown (Haataja et al., 1994; Sonninen et al., 1999; Varho et al., 2000; Parazzini et al., 2003; Morse et al., 2005; Steenweg et al., 2010). The process of myelination comprises a sequence of intricate developmental events that start by oligodendrocyte progenitors (OPs) proliferating in the ventral part of the embryonic neural tube (Baumann and Pham-Dinh, 2001; Miller, 2002; Miller, 2005; Kessaris et al., 2006; Bercury and Macklin, 2015). These OPs subsequently migrate dorsally and rostrally throughout the forebrain and spinal cord, contact axons, and differentiate into myelin-forming oligodendrocytes (OLs). The OL lineage is generally divided into four stages: early OPs, preoligodendrocytes or late OPs, immature OL and mature OL. Craig et al. (2003) studied the analogy of human and rodent OL lineage progression. Their quantification of these events in rodents revealed that cerebral white matter mainly contains late OPs at postnatal day 2 (p2), whereas immature OLs remain a minority (Craig et al., 2003). Later (around p7), immature OLs become the majority and initiate myelination.

Sialin-deficient mice were generated to study the pathophysiological mechanisms of clinical SASD (Prolo et al., 2009; Moechars et al., 2005). Sialin deficiency was indeed shown to cause hypomyelination in these mice, which was attributed to defective OL lineage maturation, leading to cell death and functional defects. Clinical SASD studies showed that functional capacities of patients were related to their levels of residual sialin activity (Wreden et al., 2005; Ruivo et al., 2008). In the present report, we further detailed the various histopathological features of postnatal progressive leukoencephalopathy in sialin-deficient mice, and assessed their functional consequences. Genetic and histological time-course expression of myelin, OL lineage and other pathogenically relevant markers was examined during postnatal brain development. Finally, we identified milestones of neurobehavioral development in mouse pups to document potential developmental disabilities caused by their sialin deficiency. Our results provide new insights on the pathophysiological mechanisms of SASD hypomyelination and could contribute to therapeutic strategies in these and more common myelination disorders.

2. Results

2.1. *Slc17a5*$^{-/-}$ mice show a progressive disease course and premature mortality

The *Slc17a5*$^{-/-}$ mice were first presented in 2005 (Moechars et al., 2005) and have been previously characterized (Prolo et al., 2009). Our qualitative observations of these mice have been consistent with their published phenotype i.e. they experience growth delays, making them smaller than equivalently aged controls, and they had a severely reduced lifespan.

2.2. *Slc17a5*$^{-/-}$ mice show free sialic acid accumulation and defective lysosomal transport

SASD results from defective clearance of free sialic acid out of the lysosome via the lysosomal transport protein sialin. To determine the level to which *Slc17a5*$^{-/-}$ mice mimic biochemical characteristics of clinical SASD, the amount of free sialic acid in embryonic fibroblasts of *Slc17a5*$^{+/+}$, *Slc17a5*$^{+/-}$ and *Slc17a5*$^{-/-}$ mice was first compared with diagnostic values of cultured fibroblasts of all clinical variants of SASD patients (ISSD, intermediate SASD and Salla disease; Fig. 1A). *Slc17a5*$^{-/-}$ mice showed an accumulation of free sialic acid (66 nmol/mg protein) in fibroblast homogenates, exceeding the most severe clinical phenotype ISSD (30 nmol/mg protein).

Next, we confirmed that these elevated levels could indeed be linked to defective sialin-mediated lysosomal clearance. Proton-gradient mediated transport, featuring tritiated glucuronic acid as a sialin substrate, was assessed using purified lysosomal membrane vesicles from livers of rat (RLV), *Slc17a5*$^{+/+}$, *Slc17a5*$^{+/-}$ and *Slc17a5*$^{-/-}$ mice. Increased

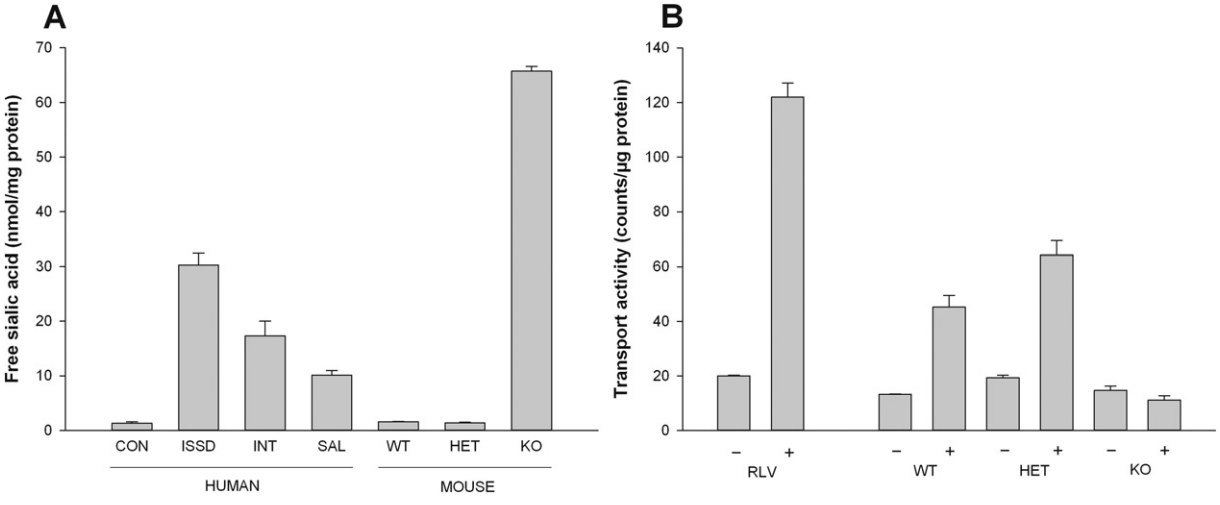

Fig. 1. Biochemical characteristics of sialin-deficient mice. (A) Concentration of free sialic acid in cultured fibroblasts of *Slc17a5*$^{+/+}$ mouse (WT), *Slc17a5*$^{+/-}$ mouse (HET) and *Slc17a5*$^{-/-}$ mouse (KO). For comparison free sialic acid was also measured in human skin fibroblasts from controls (CON) and the three clinical variants of SASD, infantile (ISSD), intermediate (INT) and Salla (SAL) type. (B) Transport activity of sialin in purified lysosomal membrane vesicles of mouse livers. Uptake of radiolabeled glucuronic acid in WT, HET and KO mice was evaluated. Activity was measured in the presence (+) and in the absence (−) of a proton gradient. As reference, activity was also measured in rat liver vesicles (RLV). Data are presented as mean + SEM.

uptake of glucuronic acid was observed in rat as well as *Slc17a5*$^{+/+}$ and *Slc17a5*$^{+/-}$ mouse vesicles upon acidification of the environment (+) (Mancini et al., 1989). However, lysosomal vesicles prepared from *Slc17a5*$^{-/-}$ mice showed completed absence of increased substrate-uptake (− versus +), confirming defective lysosomal transport through sialin (Fig. 1B).

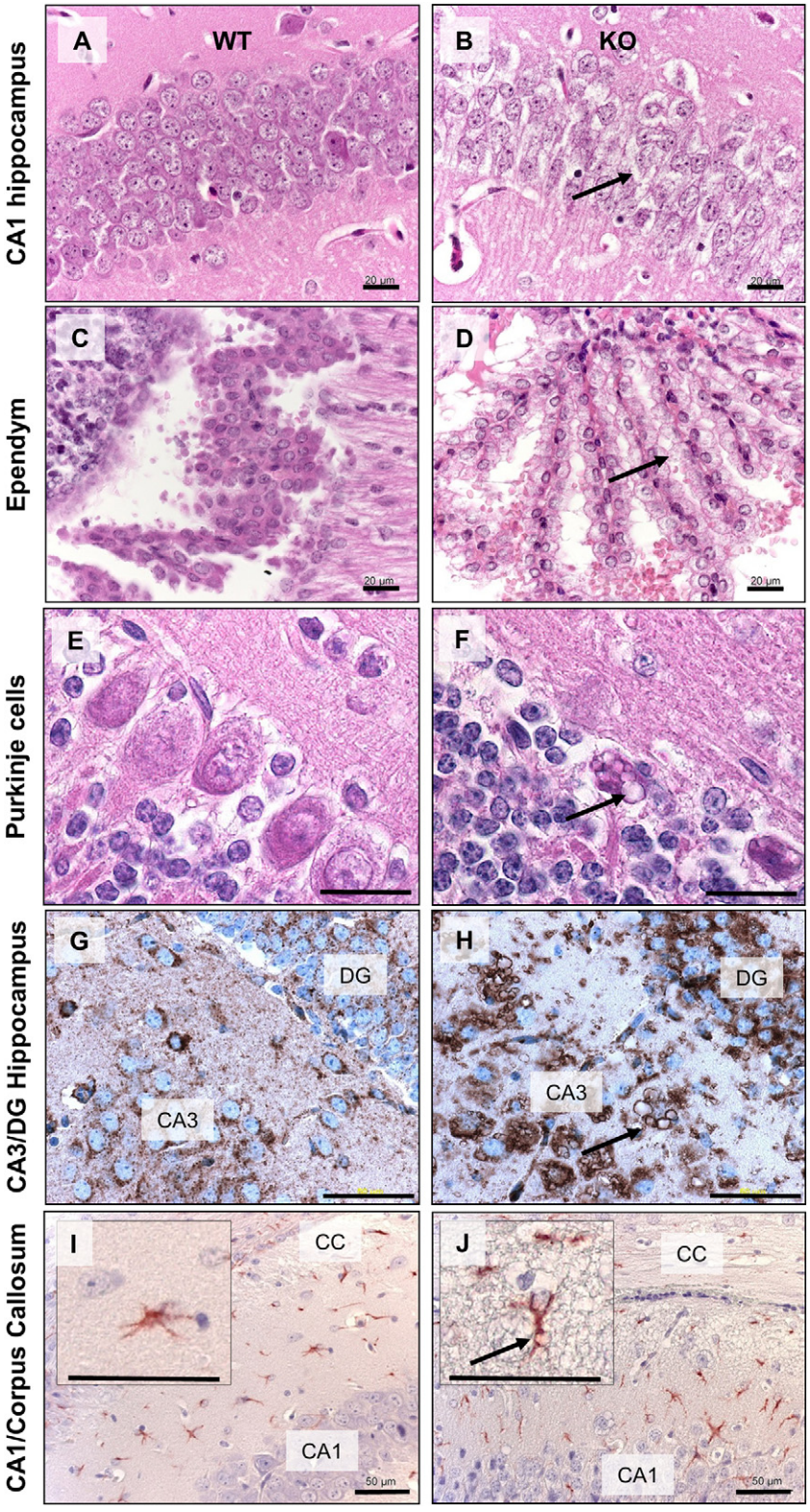

Fig. 2. Lysosomal vacuolization of CNS cells in sialin-deficient mice. CNS cells of *Slc17a5*$^{+/+}$ mice (WT, left panel) and *Slc17a5*$^{-/-}$ mice (KO, right panel) at p18. A–F: Hematoxylin-eosin staining: cytoplasmic vacuolization in CA1 hippocampal neurons (B), ependymal cells of third ventricle (D) and Purkinje cells in cerebellum (F) of *Slc17a5*$^{-/-}$ mice, in comparison to *Slc17a5*$^{+/+}$ mice (A, C, E). G–H: LAMP-1 immunohistochemistry (brown) of hippocampus dentate gyrus (DG) and CA-3 neurons: *Slc17a5*$^{+/+}$ mice show granular, punctate staining (G); *Slc17a5*$^{-/-}$ mice show irregularly shaped, prominent vacuoles positive for LAMP-1 (H: arrow). I–J: GFAP-immunohistochemistry (red) on hippocampus of *Slc17a5*$^{+/+}$ mice (I) and *Slc17a5*$^{-/-}$ mice (J). Arrow: vacuolization of cytoplasm in GFAP-immunoreactive astro-glial cell. Scale bars (A–D): 20 μm and (E–H, I–J): 50 μm. (For interpretation of the references to color in this figure legend, the reader is referred to the web version of this article.)

2.3. *Slc17a5*$^{-/-}$ mice show prominent lysosomal vacuolization in central and peripheral tissues

Intralysosomal substrate accumulation induces vacuolization in affected cells, which constitutes a typical neuropathological hallmark of human SASD as well as other lysosomal storage disorders. We investigated lysosomal storage pathology in several central and peripheral tissues. Indeed, the most prominent morphological difference observed in different types of cells (e.g.: neurons, glial cells, ependymal cells) between *Slc17a5*$^{+/+}$ and *Slc17a5*$^{-/-}$ mice (p18) throughout the entire nervous system was cytoplasmic vacuolization (Fig. 2).

Vacuolization was observed in neuronal and non-neuronal CNS cells of *Slc17a5*$^{-/-}$ mice, such as hippocampal neurons (Fig. 2B), ependymal cells (Fig. 2D), cerebellar Purkinje cells (Fig. 2F), spinal cord neurons (not shown) and astroglial cells (Fig. 2J). This was in contrast to respective CNS cells of *Slc17a5*$^{+/+}$ mice (Fig. 2A,C,E,I). LAMP-1 immunohistochemistry confirmed that these vacuolar structures are likely derived from lysosomes and/or late endosomes. LAMP-1 immunoreactivity in CA3 and dentate gyrus (DG) neurons shows a granular, punctate, distinct pattern in brain of *Slc17a5*$^{+/+}$ mice (Fig. 2G), whereas *Slc17a5*$^{-/-}$ mice show irregularly shaped, prominent vacuoles, strongly positive for LAMP-1 (Fig. 2H). Similar to CNS cells, cytoplasmic vacuolization was observed in Schwann cells of the ischiadic nerve in *Slc17a5*$^{-/-}$ mice, which however showed normal myelination (Fig. 3). Other peripheral tissue such as liver (Fig. 4B), endo-/exocrine pancreas (Fig. 4E, F) and gastro-intestinal mucosa and plexus (Fig. 4H, J) also showed signs of vacuolization in *Slc17a5*$^{-/-}$ mice. Histological evidence for neuroinflammation was observed in occurrence of reactive gliosis in the hippocampal fissure and external capsule of 3 of 5 investigated *Slc17a5*$^{-/-}$ brains at p18, as revealed by GFAP-immunofluorescence (data not shown). The GFAP-immunoreactivity appeared to be denser in *Slc17a5*$^{-/-}$ mice, for which however no quantification was performed. In general, the average number of neurons in randomly selected areas (0.096 mm^2 per area) of cerebral cortex and of Purkinje cells in randomly selected areas (0.096 mm^2 per area) of cerebellum did not differ significantly ($p = 0.52$ for cortical neuronal density & $p = 0.71$ for Purkinje cell density) between *Slc17a5*$^{+/+}$ (37.6 ± 1.8 and 23.2 ± 2 respectively) and *Slc17a5*$^{-/-}$ (38.4 ± 1.1 and 22.1 ± 2.7 respectively) mice. On average 38.0 neurons and 22.7 Purkinje cells were counted per high power microscopic field (0.096 mm^2).

2.4. *Slc17a5*$^{-/-}$ mice show progressive differential gene expression related to lysosomal dysfunction, neuroinflammation and hypomyelination during postnatal brain development

Microarray analysis was performed on total brain RNA isolated from *Slc17a5*$^{-/-}$ mice and *Slc17a5*$^{+/+}$ controls at p0, p10 and p18. This comparison was done to investigate the performance of different genes involved during postnatal brain development, providing further insight in pathogenic processes in SASD. Specific time points were chosen to include evaluation before and after onset of clinical observations. The pathways where differential gene expression is observed between genotypes are illustrated in function of time (Fig. 5). Expression of *Slc17a5* was found to be clearly down regulated in the *Slc17a5*$^{-/-}$ mice, confirming the knock down. During development an increase in the number of differently expressed genes was observed.

In brains of newborn *Slc17a5*$^{+/+}$ versus *Slc17a5*$^{-/-}$ littermates (p0), SAM analysis identified only 12 genes that were differentially expressed, 7 of which were down regulated (including: *Slc17a5* and myelin basic protein (MBP)). Like many other genes involved in CNS myelination, myelin regulatory factor (Myrf) was not differentially expressed at p0. Furthermore, no differential expression was observed for the platelet-derived growth factor-α (Pdgfra) and NG2 chondroitin sulphate proteoglycan (Cspg4). These constitute two markers of the early OP precursor cell, which is predominant at p0. Some upregulated genes are related to neuroinflammatory response (macrophage expressed gene 1 (Mpeg1) and Fcgr2b), while others include lysosomal enzymes cathepsin D and galactosylceramidase (Galc). Upregulation of lysosomal and neuroinflammatory genes are therefore among the earliest pronounced responses to sialin deficiency in *Slc17a5*$^{-/-}$ mice.

SAM analysis (FDR < 0.005) on the microarray data of the brain of *Slc17a5*$^{-/-}$ mice compared to *Slc17a5*$^{+/+}$ mice at p10 and p18 demonstrated a substantial increase and striking overlap of differentially expressed genes, albeit effects appeared more subtle at p10 (Fig. 5). At p18, 378 genes were differentially expressed in brain samples of *Slc17a5*$^{+/+}$ versus *Slc17a5*$^{-/-}$ mice. Expression of 298 of them was found to be downregulated in the brain of *Slc17a5*$^{-/-}$ mice compared to *Slc17a5*$^{+/+}$ mice. Only 20% of the significantly altered genes were upregulated. Increased differential expression of several genes that encode lysosomal enzymes and other lysosomal related proteins was indicative of lysosomal dysregulation in the brain of *Slc17a5*$^{-/-}$ mice. A multitude

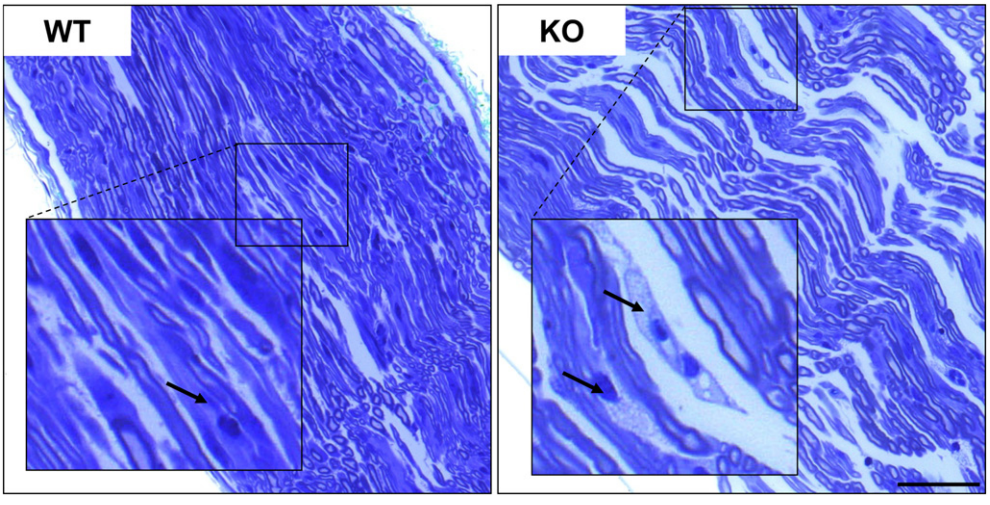

Fig. 3. Cytoplasmic vacuolization but normal myelination in the PNS of sialin-deficient mice. Toluidine blue staining of a longitudinal section of plastic embedded nervus ischiadicus. The peripheral nerve fibers of *Slc17a5*$^{+/+}$ mice (WT, A) and of *Slc17a5*$^{-/-}$ mice (KO, B) have a similar number and thickness at p18. Schwann cells in nerve fibers (arrow) of *Slc17a5*$^{-/-}$ (B) contain cytoplasmic vacuoles whereas this was not observed in Schwann cells of peripheral nerve fibers from *Slc17a5*$^{+/+}$ mice (A). Scale bars: 50 μm. (For interpretation of the references to color in this figure legend, the reader is referred to the web version of this article.)

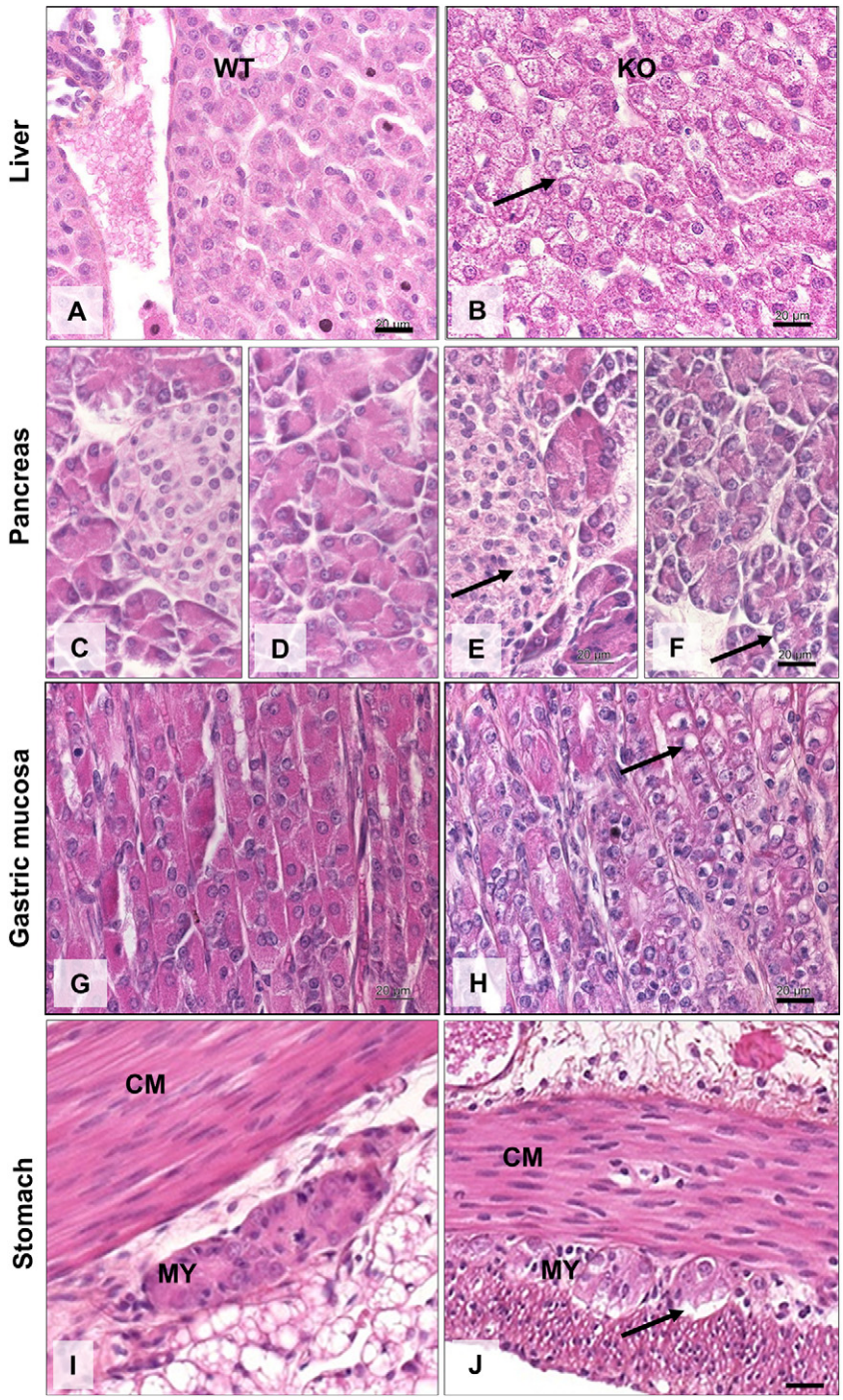

Fig. 4. Lysosomal vacuolization of different cell types in peripheral tissues in sialin-deficient mice. Hematoxylin-eosin staining of peripheral tissues of *Slc17a5*$^{+/+}$ mice (WT, left panel), *Slc17a5*$^{-/-}$ mice (KO, right panel) at P18. Arrows indicate vacuolization which was observed in liver (B), endocrine pancreas (E), exocrine pancreas (F), gastric mucosa (H) and gastric myenteric plexus (J) of *Slc17a5*$^{-/-}$ mice in contrast to corresponding peripheral tissues of *Slc17a5*$^{+/+}$ mice (A,C,D,G,I).

of upregulated genes pointed to a progressive neuroinflammatory response with a notable increased presence of activated phagocytic macrophages (Mpeg1). SAM analysis also identified other genes involved in cholesterol and lipid biosynthesis to be differentially expressed in the brain of *Slc17a5*$^{-/-}$ mice, mainly at reduced levels. Expression of many known genes encoding constituents of myelin, the compact lamellar wrapping found on relative large fiber axons, was decreased. Examples of these are MBP, myelin-associated oligodendrocytic basic protein (Mopb), myelin-associated glycoprotein (Mag), cyclic nucleotide phosphodiesterase 1 (Cnp1), proteolipid protein 1 (Plp1), and oligodendrocyte-myelin glycoprotein (Omg). Genes that encode typical markers of OL lineage, the neural tube derived cells that form myelin,

Fig. 5. Genes encoding typical markers of the oligodendrocyte lineage are downregulated in sialin-deficient mice. Gene expression analysis in mouse brain at p0, p10 and p18 showing main affected processes when comparing *Slc17a5*$^{-/-}$ to *Slc17a5*$^{+/+}$ mice. The genes listed are those that show at least 20% change for at least one of the three time points. Differential expression is shown as bars representing the log2ratios. Bars to the left represent genes down regulated in *Slc17a5*$^{-/-}$ mice. Bars reaching the outer grey lines represent genes with > 4-fold change. Bars smaller than the grey background zone show <2-fold change.

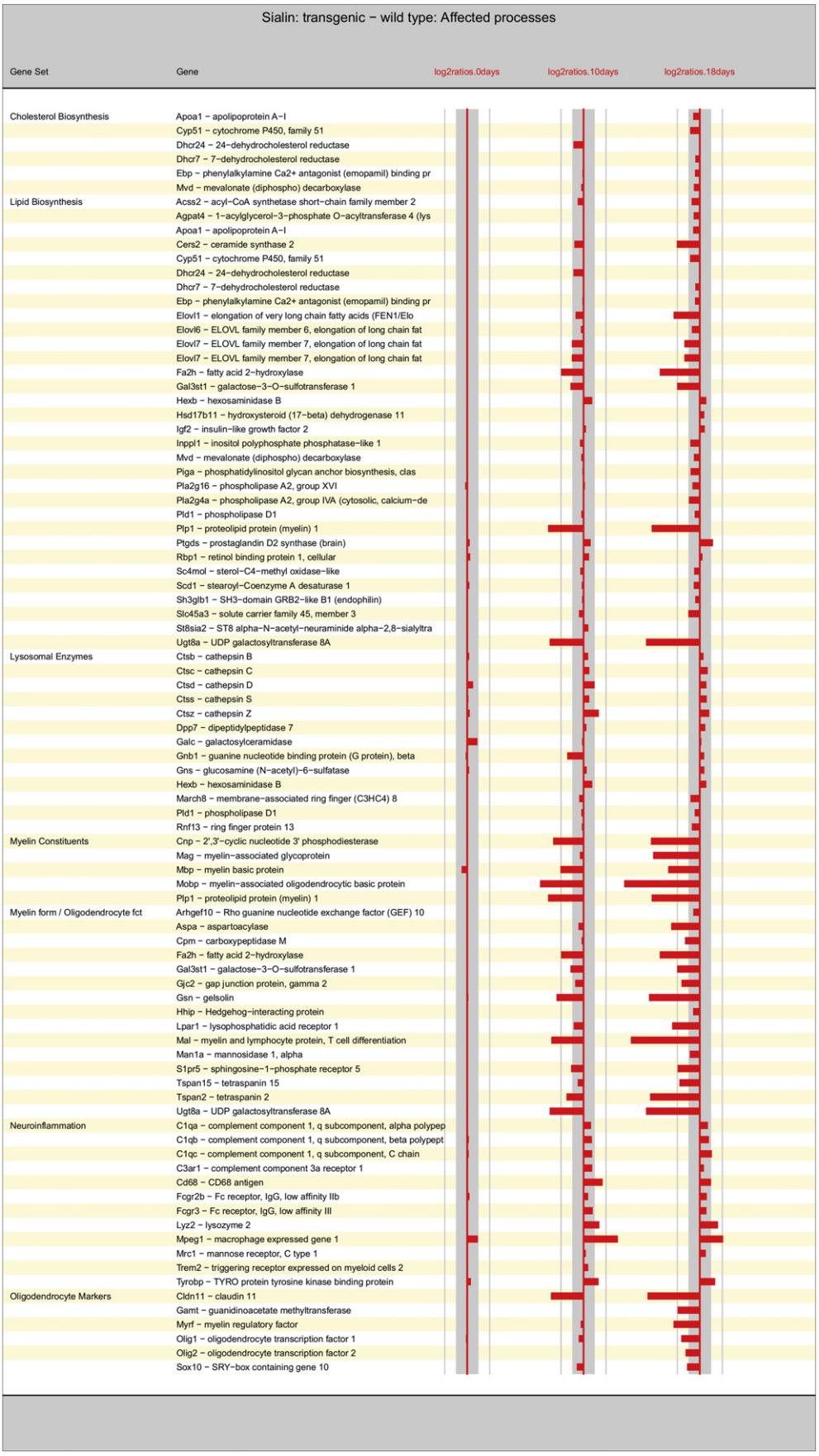
Sialin: transgenic − wild type: Affected processes
Gene Set
Gene
log2ratios.0days
log2ratios.10days
log2ratios.18days
Cholesterol Biosynthesis
Apoa1 − apolipoprotein A−I
Cyp51 − cytochrome P450, family 51
Dhcr24 − 24−dehydrocholesterol reductase
Dhcr7 − 7−dehydrocholesterol reductase
Ebp − phenylalkylamine Ca2+ antagonist (emopamil) binding pr
Mvd − mevalonate (diphospho) decarboxylase
Lipid Biosynthesis
Acss2 − acyl−CoA synthetase short−chain family member 2
Agpat4 − 1−acylglycerol−3−phosphate O−acyltransferase 4 (lys
Apoa1 − apolipoprotein A−I
Cers2 − ceramide synthase 2
Cyp51 − cytochrome P450, family 51
Dhcr24 − 24−dehydrocholesterol reductase
Dhcr7 − 7−dehydrocholesterol reductase
Ebp − phenylalkylamine Ca2+ antagonist (emopamil) binding pr
Elovl1 − elongation of very long chain fatty acids (FEN1/Elo
Elovl6 − ELOVL family member 6, elongation of long chain fat
Elovl7 − ELOVL family member 7, elongation of long chain fat
Elovl7 − ELOVL family member 7, elongation of long chain fat
Fa2h − fatty acid 2−hydroxylase
Gal3st1 − galactose−3−O−sulfotransferase 1
Hexb − hexosaminidase B
Hsd17b11 − hydroxysteroid (17−beta) dehydrogenase 11
Igf2 − insulin−like growth factor 2
Inppl1 − inositol polyphosphate phosphatase−like 1
Mvd − mevalonate (diphospho) decarboxylase
Piga − phosphatidylinositol glycan anchor biosynthesis, clas
Pla2g16 − phospholipase A2, group XVI
Pla2g4a − phospholipase A2, group IVA (cytosolic, calcium−de
Pld1 − phospholipase D1
Plp1 − proteolipid protein (myelin) 1
Ptgds − prostaglandin D2 synthase (brain)
Rbp1 − retinol binding protein 1, cellular
Sc4mol − sterol−C4−methyl oxidase−like
Scd1 − stearoyl−Coenzyme A desaturase 1
Sh3glb1 − SH3−domain GRB2−like B1 (endophilin)
Slc45a3 − solute carrier family 45, member 3
St8sia2 − ST8 alpha−N−acetyl−neuraminide alpha−2,8−sialyltra
Ugt8a − UDP galactosyltransferase 8A
Lysosomal Enzymes
Ctsb − cathepsin B
Ctsc − cathepsin C
Ctsd − cathepsin D
Ctss − cathepsin S
Ctsz − cathepsin Z
Dpp7 − dipeptidylpeptidase 7
Galc − galactosylceramidase
Gnb1 − guanine nucleotide binding protein (G protein), beta
Gns − glucosamine (N−acetyl)−6−sulfatase
Hexb − hexosaminidase B
March8 − membrane−associated ring finger (C3HC4) 8
Pld1 − phospholipase D1
Rnf13 − ring finger protein 13
Myelin Constituents
Cnp − 2',3'−cyclic nucleotide 3' phosphodiesterase
Mag − myelin−associated glycoprotein
Mbp − myelin basic protein
Mobp − myelin−associated oligodendrocytic basic protein
Plp1 − proteolipid protein (myelin) 1
Myelin form / Oligodendrocyte fct
Arhgef10 − Rho guanine nucleotide exchange factor (GEF) 10
Aspa − aspartoacylase
Cpm − carboxypeptidase M
Fa2h − fatty acid 2−hydroxylase
Gal3st1 − galactose−3−O−sulfotransferase 1
Gjc2 − gap junction protein, gamma 2
Gsn − gelsolin
Hhip − Hedgehog−interacting protein
Lpar1 − lysophosphatidic acid receptor 1
Mal − myelin and lymphocyte protein, T cell differentiation
Man1a − mannosidase 1, alpha
S1pr5 − sphingosine−1−phosphate receptor 5
Tspan15 − tetraspanin 15
Tspan2 − tetraspanin 2
Ugt8a − UDP galactosyltransferase 8A
Neuroinflammation
C1qa − complement component 1, q subcomponent, alpha polypep
C1qb − complement component 1, q subcomponent, beta polypept
C1qc − complement component 1, q subcomponent, C chain
C3ar1 − complement component 3a receptor 1
Cd68 − CD68 antigen
Fcgr2b − Fc receptor, IgG, low affinity IIb
Fcgr3 − Fc receptor, IgG, low affinity III
Lyz2 − lysozyme 2
Mpeg1 − macrophage expressed gene 1
Mrc1 − mannose receptor, C type 1
Trem2 − triggering receptor expressed on myeloid cells 2
Tyrobp − TYRO protein tyrosine kinase binding protein
Oligodendrocyte Markers
Cldn11 − claudin 11
Gamt − guanidinoacetate methyltransferase
Myrf − myelin regulatory factor
Olig1 − oligodendrocyte transcription factor 1
Olig2 − oligodendrocyte transcription factor 2
Sox10 − SRY−box containing gene 10

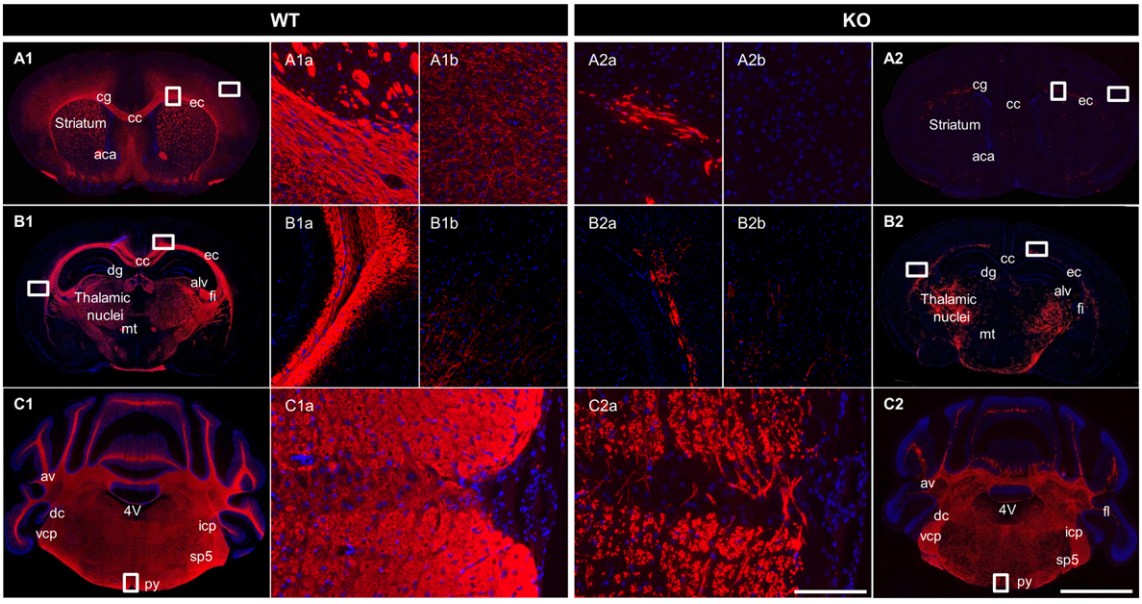

Fig. 6. Gradual decrease of CNS myelination from cerebellar to frontal regions in sialin-deficient mice. MBP immunofluorescence in CNS of *Slc17a5*$^{+/+}$ (WT, left panel) and *Slc17a5*$^{-/-}$ mouse brain (KO, right panel) at p18. A marked decrease and abnormal pattern of MBP staining in CNS of *Slc17a5*$^{-/-}$ mice is observed in coronal sections from frontal brain regions (A2), midbrain (B2) and cerebellum (C2). The loss of myelin in white matter of *Slc17a5*$^{-/-}$ mouse brains is most pronounced in frontal and midbrain regions. High magnification images of MBP immunofluorescence (middle panels) from indicated areas of corpus callosum, cerebral cortex and cerebellum of *Slc17a5*$^{+/+}$ (WT: A1a, B1a - A1b, B1b - C1a) and *Slc17a5*$^{-/-}$ mouse brain (KO: A2a, B2a - A2b, B2b – C2a). Red: MBP-IF; blue: Hoechst nuclear counter stain. 4V: 4th ventricle, aca: anterior commissure, alv: alveus of the hippocampus, av.: arbor vitae cerebellum, cc: corpus callosum, cg: cingulum, dc: dorsal cochlear nucleus, dg: dentate gyrus, ec: external capsule, fi: fimbria, fl: flocculus, icp: inferior cerebellar peduncle, mt: mammilothalamic tract, py: pyramidal tract, sp5: spinal trigeminal tract, vcp: ventral cerebellar peduncle. Scale bars: 200 μm (high magnifications), 2000 μm (overviews). (For interpretation of the references to color in this figure legend, the reader is referred to the web version of this article.)

were also found to be expressed at reduced levels in the brain of *Slc17a5*$^{-/-}$ mice. Expression of Myrf, a transcription factor which directly regulates differentiation of OLs and their expression of myelin genes was downregulated at p18. Apart from these markers, a wide variety of genes expressed predominantly or exclusively in the OLs or reported to be involved in myelin formation or OL function were also found to be expressed at reduced levels in the brain of *Slc17a5*$^{-/-}$ mice. The observed decreased expression of such a wide variety of OL and myelin marker genes points to a strong reduction in the number of mature OLs in the brain of the sialin-deficient mouse.

2.5. Slc17a5$^{-/-}$ *mice show a distinct spatiotemporal pattern of CNS hypomyelination*

In relation to the progressive downregulation of OL and myelin marker genes during postnatal brain development, we investigated age- and region-specific CNS myelination patterns in *Slc17a5*$^{-/-}$ mice. In contrast to PNS observations, myelination of CNS nerve fibers proved obviously decreased in *Slc17a5*$^{-/-}$ mice. In *Slc17a5*$^{+/+}$ brains from p18 mice, immunofluorescence of the myelin constituent MBP labeled all nerve tracts as is illustrated in Fig. 6 (A1, B1, C1). In *Slc17a5*$^{-/-}$ mice, MBP staining was markedly decreased or even absent in nerve fiber tracts in all investigated brain regions. The decreased and altered MBP immunoreactivity in the CNS of *Slc17a5*$^{-/-}$ mice showed a prominent difference between frontal brain regions and (ventral) hind brain/cerebellum (Fig. 6A2, B2, C2). The most affected cerebral regions include corpus callosum (Fig. 6A2a-B2a) as well as cingulum, internal and external capsule and most large white matter fiber tracts in the CNS. MBP immunoreactivity was nearly absent in cerebral cortex (Fig. 6A2b-B2b). The remaining MBP-labeling, especially present in dorsal parts of capsula, striatum and larger nerve fibers was variable and had an aberrant clumpy and disorganized pattern in *Slc17a5*$^{-/-}$ mice brain (see also Fig. 7).

To investigate the integrity of nerve fiber axons, central brain regions of *Slc17a5*$^{+/+}$ and *Slc17a5*$^{-/-}$ mice were stained for neurofilament (70 and 200 kDa). Data showed that axons were still present in most nerve fiber tracts of *Slc17a5*$^{-/-}$ mice (not in anterior commissure, see Fig. 6A2, Fig. 7). Globoid structures (Fig. 8 middle and lower panel) were present in the affected white matter of cerebrum and cerebellum of *Slc17a5*$^{-/-}$ mice and these showed strong neurofilament immunoreactivity. Double labeling immunofluorescence staining of neurofilament and MBP showed clear engulfment of these axonal swellings by fragmented MBP (Fig. 8 middle panel).

To gain further insight in temporal patterns of CNS myelination, we investigated markers of OL lineage cells in *Slc17a5*$^{-/-}$ mice brain during the myelination period (Fig. 9A). We used three different markers of OL lineage maturation and followed the myelination process through days p2, p7 and p11 in *Slc17a5*$^{+/+}$ and *Slc17a5*$^{-/-}$ mice. While O1 and O4 markers both stain immature OL, O4 is also a marker for late OPs (Craig et al., 2003). MBP was used as a marker for myelinating, mature OL.

Shortly after birth, the staining of OPs did not seem to be strikingly different between *Slc17a5*$^{+/+}$ and *Slc17a5*$^{-/-}$ mice, as shown by O4 staining at p2, and was mostly visible in ventral reticular brainstem regions. In *Slc17a5*$^{+/+}$ mice, the MBP, O4 and O1 staining progressively diffused through p7 and p11 from the central white matter areas to cerebral cortical areas, capsula interna and externa and corpus callosum. However, while the pool of OPs as well as maturing OLs weakly increased in brain of *Slc17a5*$^{-/-}$ mice, as seen by staining at p7 and p11 for the different OL lineage markers, it remained localized in central brainstem areas and was weakly present in cerebellar white matter (Fig. 9B).

2.6. Slc17a5$^{-/-}$ *mice show progressive delay of neurobehavioral development*

Finally, we assessed neurobehavioral development of *Slc17a5*$^{-/-}$ mice to characterize the functional consequences of the observed genetic and pathological alterations. Achievement of developmental milestones (Fig. 10) and performance level for some of these behaviors (Fig. 11) was assessed from p1 to p21. Early milestone behaviors include negative geotaxis (turning the body head up when placed head down

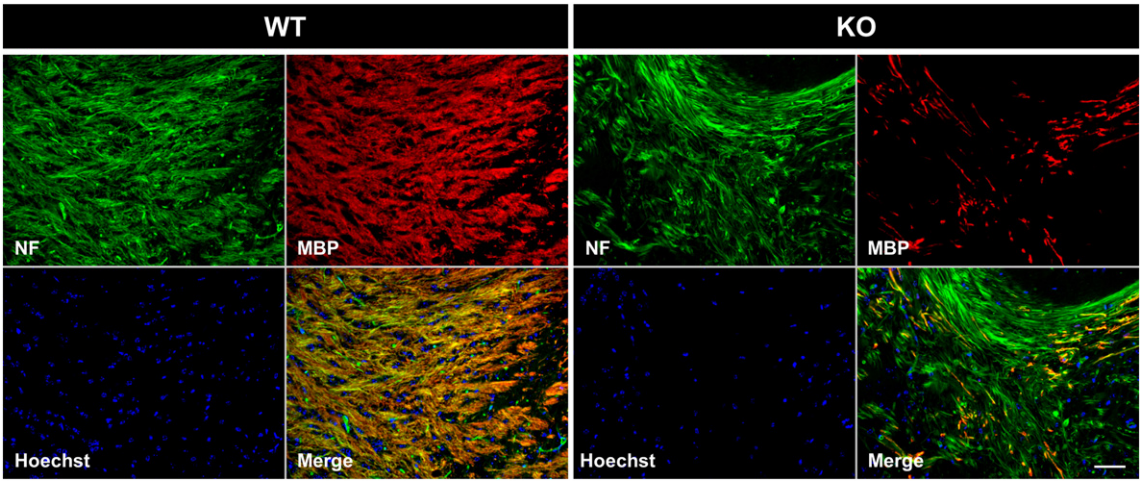

Fig. 7. Decreased myelination but limited axonal loss in central brain regions of sialin-deficient mice. Immunofluorescence double labeling of MBP (red) and neurofilament (green) in internal capsular region of *Slc17a5*$^{+/+}$ (WT, left) and *Slc17a5*$^{-/-}$ (KO, right) mouse brain at p18 (bregma −3.30, interaural 5.70 mm) (Paxinos and Watson, 1986). (Axon: green, myelin sheet: red, blue: Hoechst nuclear counter stain). Scale bars: 50 μm. (For interpretation of the references to color in this figure legend, the reader is referred to the web version of this article.)

on an incline), cliff aversion (crawling away when placed at an edge) and surface righting (righting the body when placed on the back). These behaviors reflect a postural reflex in response to altered body orientation as well as physical strength and coordinated movement. *Slc17a5*$^{-/-}$ mice showed similar performance to control littermates in negative geotaxis and cliff aversion (Fig. 10; Fig. 11A–B). Milestone criterion for surface righting was also reached at the same time (Fig. 10), although performance speed was lower, especially during the first perinatal and neonatal days (Fig. 11C; main effect of genotype; $p < 0.01$). All later-stage motor and sensory milestones were significantly retarded in these mice (Fig. 10). Tactile ear twitch reflexes were delayed ($p < 0.01$), while auditory startle responses were completely absent ($p < 0.001$). Their weak appearance was illustrated by a delayed ability of forelimb grasping ($p < 0.05$). Strong effects were also observed for the late postnatal motor milestones of locomotion development ($p < 0.001$) and air righting (righting the body after being held upside down and released; $p < 0.001$). Time to exit the circle during the locomotion test was significantly higher in *Slc17a5*$^{-/-}$ mice ($p < 0.001$), although differences were less pronounced for p8 (post-hoc $p < 0.05$), p9 ($p < 0.01$) and p16 ($p < 0.05$) (Fig. 11D; main effect of genotype, $p < 0.001$; interaction of day and genotype, $p < 0.05$). Late-stage motor impairment was further quantified using an open field test at the age of 6–7 weeks. Comparing *Slc17a5*$^{-/-}$ mice to *Slc17a5*$^{+/+}$ littermates a significant reduction in both the distance traveled (2081 ± 561 cm versus 482 ± 524 cm; $p < 0.001$) and rearing (35 ± 28 versus 2 ± 2; $p < 0.05$) was observed in the *Slc17a5*$^{-/-}$ mutants.

3. Discussion

Sialin-deficient mice were generated to study the pathophysiology of clinical SASD (Prolo et al., 2009; Moechars et al., 2005). Sialin deficiency induced free sialic acid accumulation in these mice, and mimicked SASD-related leukoencephalopathy and clinical ISSD. Proton-gradient mediated transport of glucuronic acid was deficient in lysosomal vesicles from *Slc17a5*$^{-/-}$ mice, confirming defective sialin-mediated transport. Free sialic acid accumulated in cultured *Slc17a5*$^{-/-}$ mouse fibroblasts, and vacuolization with strong lysosomal marker LAMP-1 immunoreactivity occurred in all examined tissues (including CNS and PNS). These observations confirm that *Slc17a5*$^{-/-}$ mice reproduce the basic pathogenic events of the human disorder. In the present report, we examined the occurrence of pathognomonic genetic, histopathological and behavioral anomalies in this putative ISSD model. An overview of the overall set of findings can be found in Fig. 12.

Hypomyelination is a typical pathological and neuroradiological finding in brain of SASD patients (Haataja et al., 1994; Sonninen et al., 1999; Varho et al., 2000; Parazzini et al., 2003; Morse et al., 2005; Steenweg et al., 2010). Even in mildly affected Salla disease patients, cerebral hypomyelination seems to be the most consistent abnormality, observed already at the age of 3 to 6 months, well before the first neurological symptoms occur (Sonninen et al., 1999; Biancheri et al., 2002). Severe hypomyelination in cerebral and cerebellar white matter has been reported from birth in ISSD patients, consistent with prenatally arrested myelination (Parazzini et al., 2003). Hypomyelination appears to be a consequence of insufficient myelin deposition in sialin-deficient mice as well. Brains of *Slc17a5*$^{-/-}$ mice were examined histologically at an age at which the myelination process is still ongoing (p18). Strongly reduced myelin staining indicated defective myelination, which appears related to a reduction of mature and possibly immature OLs. Microarray analyses further indicated that, already at p10 and markedly at p18, expression of a wide variety of OL and myelin marker genes was reduced in *Slc17a5*$^{-/-}$ mice, consistent with a strong reduction of mature OL. For example, *Myrf* expression was unchanged at p0 but downregulated at p10 and p18 in *Slc17a5*$^{-/-}$ mice. Notably, the transcription factor *Myrf* is crucial for OL maturation and subsequent myelination processes (Emery et al., 2009). It was shown to be decreased in the mouse model for Niemann-Pick Type C1 disease (Yan et al., 2011), another lysosomal storage disorder characterized by perturbed myelination. In perinatal mice, *Myrf* expression by myelinating OLs is limited to the spinal cord and posterior brain regions (Emery et al., 2009). This supports initial normal myelination in caudal CNS regions of *Slc17a5*$^{-/-}$ mice.

Histological analysis at p18 indeed showed a gradient of OL density with highest numbers in ventral hindbrain, followed by midbrain, and forebrain SVZ, further decreasing in more distant areas. Oligodendrogenesis is a late-stage process in brain development (El Waly et al., 2014). Directed OP migration and differentiation are still ongoing in the first postnatal weeks and are essential for myelin formation. Immunohistochemistry indicated impaired colonization by immature OPs (O1+ and O4+) and consequently mature OL (MBP+) during later neonatal stages, whereas no obvious differences were observed in central brainstem areas shortly after birth (p2). The reduced O4 distribution from posterior to rostral brain regions may suggest a contribution of defective late OP migration to the observed hypomyelination. Expression of early OL precursor markers such as *Pdgfra* and *Cspg4* did however not change during postnatal brain development, in line with previous immunohistochemical findings

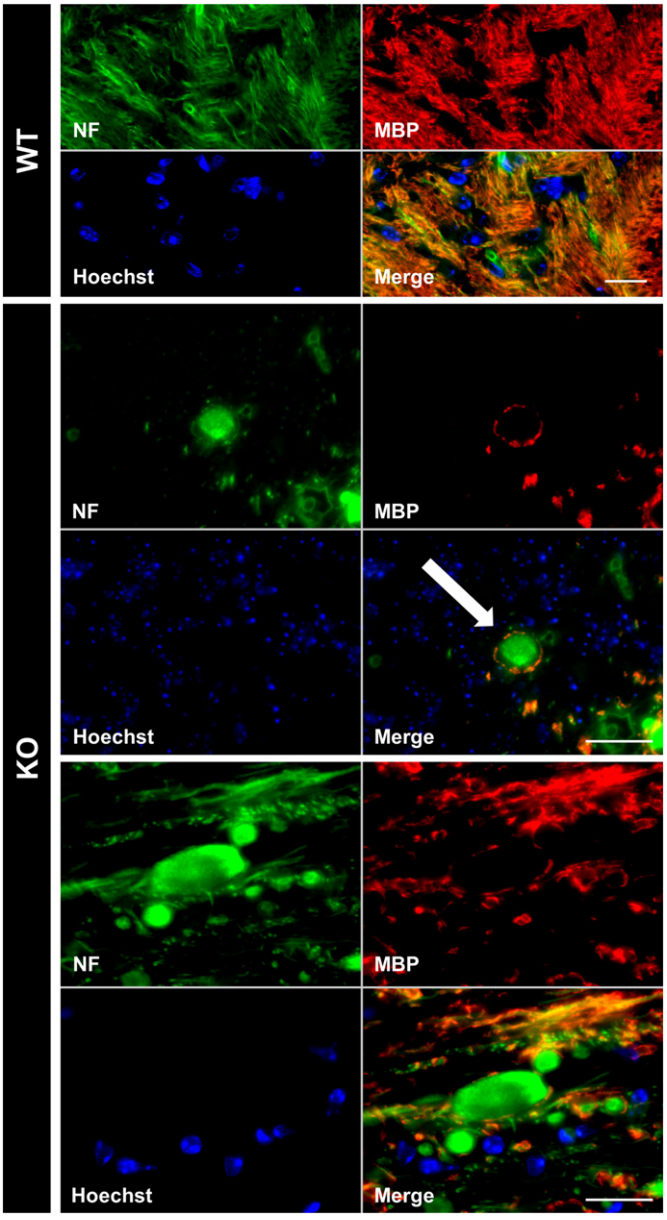

Fig. 8. Sialin-deficient mice show neuroaxonal dystrophy characterized by axonal swellings in the affected white matter. High magnification images (63×, 100×) of Immunofluorescence double labeling of MBP (red) and neurofilament (green) in cerebellum of *Slc17a5*$^{+/+}$ (WT, upper panel) and *Slc17a5*$^{-/-}$ (KO, middle and lower panel) mouse. (Axon: green, myelin sheet: red, blue: Hoechst nuclear counter stain; arrow: axonal swelling). Scale bars: 20 μm. (For interpretation of the references to color in this figure legend, the reader is referred to the web version of this article.)

(Prolo et al., 2009). Early OPs represent the major migratory stage of the OL lineage and transition to late OPs is accompanied by a substantial reduction in migratory capacity (Warrington et al., 1993; Barateiro and Fernandes, 2014). Notably, performance of a neurosphere in vitro assay on neural stem cells of sialin-deficient mice could be an interesting suggestion for future research. This could further elucidate the involvement of sialin in the different steps of the generation of myelinating oligodendrocytes.

Likewise, microarray analyses at p0 could provide more information on the early stages of pathogenesis. In contrast to the pronounced reduction in expression of myelin and OL marker genes at late developmental stages, few genes were differentially expressed at p0. Microarray analysis showed early upregulation and progressive differential expression of lysosomal genes, indicating changes in lysosomal structure and function, probably in response to accumulating storage. Increases in lysosomal size and number, and consequently also lysosomal proteins are common observations in lysosomal storage disorders (Malone, 1976). In addition, a small subset of inflammatory genes was already upregulated at this stage, suggesting an inflammatory response that preceded reduced myelination. Substantially more inflammatory genes became upregulated later in development, evident of progressive neuroinflammation in sialin-deficient mice. Progressive neuroinflammation is frequently observed in lysosomal storage disorders and could amplify hypomyelination by eliciting apoptosis (Fletcher et al., 1812). Increased cell death and impaired downregulation of polysialylated neural cell-adhesion molecule (PSA-NCAM) were observed in optic nerves of *Slc17a5*$^{-/-}$ mice, and postulated to underlie impaired myelination (Prolo et al., 2009). Developing oligodendrocytes and late OPs in particular were shown to be increasingly vulnerable to inflammatory and other insults (Back et al., 2002; Deng, 2010; Falahati et al., 2013), suggesting a substantial contribution of neuroinflammation to the apparent defect of *Slc17a5*$^{-/-}$ mice in transition of early to late OPs and more mature cells in the OL lineage.

In addition, we investigated the degree to which CNS hypomyelination and leukoencephalopathy in *Slc17a5*$^{-/-}$ mice affected their neurobehavioral performance. *Slc17a5*$^{-/-}$ mice seem to model clinical ISSD, which is characterized by severe functional impairments and developmental delays (Lemyre et al., 1999). At a rather late stage of their disease, sialin-deficient mice displayed reduced ambulation in the open field test, which might at least partly relate to the gait abnormalities described in these mice (Prolo et al., 2009). We did not observe any gross abnormalities in cerebellar development, but focal axonal swellings were observed at p18 throughout the cerebellum, which are indicative for impaired axonal transport and fiber degeneration (Prolo et al., 2009; Lovell and Jones, 1985; Kaartinen et al., 1996; Suzuki, 2003) and considered an important factor in generating movement disorders in lysosomal storage diseases (Walkley et al., 2010).

Slc17a5$^{-/-}$ mice showed a progressive delay of milestone achievement that paralleled the course of their leukoencephalopathy. They showed timely achievement of early milestones (cliff aversion, negative geotaxis and surface righting), whereas surface righting performance was impaired. The righting reflex, which depends on vestibular system and brainstem integrity, appears intact in *Slc17a5*$^{-/-}$ mice, but its execution could be more difficult depending on the postural adjustment required. Notably, myelination (especially in brainstem) was not severely affected during the early perinatal days, but declined later on. Additionally, these mice displayed severe delays in reaching the developmental milestone of air righting, also reliant on labyrinthine function, but requiring further maturation of the motor coordination system (Altman and Sudarshan, 1975). In addition, *Slc17a5*$^{-/-}$ mice showed delayed forelimb grasping as well as retarded transition from pivoting to crawling, indicating delayed maturation of hindlimb use. Moreover, they never reached the same level of straightforward locomotion as littermate controls, typical of later developmental stages. By and large, the aberrant neuromotor development in *Slc17a5*$^{-/-}$ mice seems to parallel the spatiotemporal progression of their leukoencephalopathy, supporting a causal role of defective myelinogenesis and central hypomyelination in SASD-induced motor defects. Delayed development of motor skills and/or ataxia are also typical in other human genetic hypomyelination disorders such as Pelizaeus-Merzbacher disease (Regis et al., 2008) and vanishing white matter disease (van der Lei et al., 2010), as well as in animal models of central hypomyelination such as shiverer mutant mice (Low et al., 2009). Notably, some functional impairments of sialin-deficient mice, such as their delayed tactile ear twitch reflex, could also be attributed to somatosensory defects. Also at the sensory level, *Slc17a5*$^{-/-}$ mice developed no auditory startle responses during the measured timeframe. Auditory impairment indeed appears to be another characteristic consequence of central myelination defects. For example, delayed auditory evoked potentials were observed

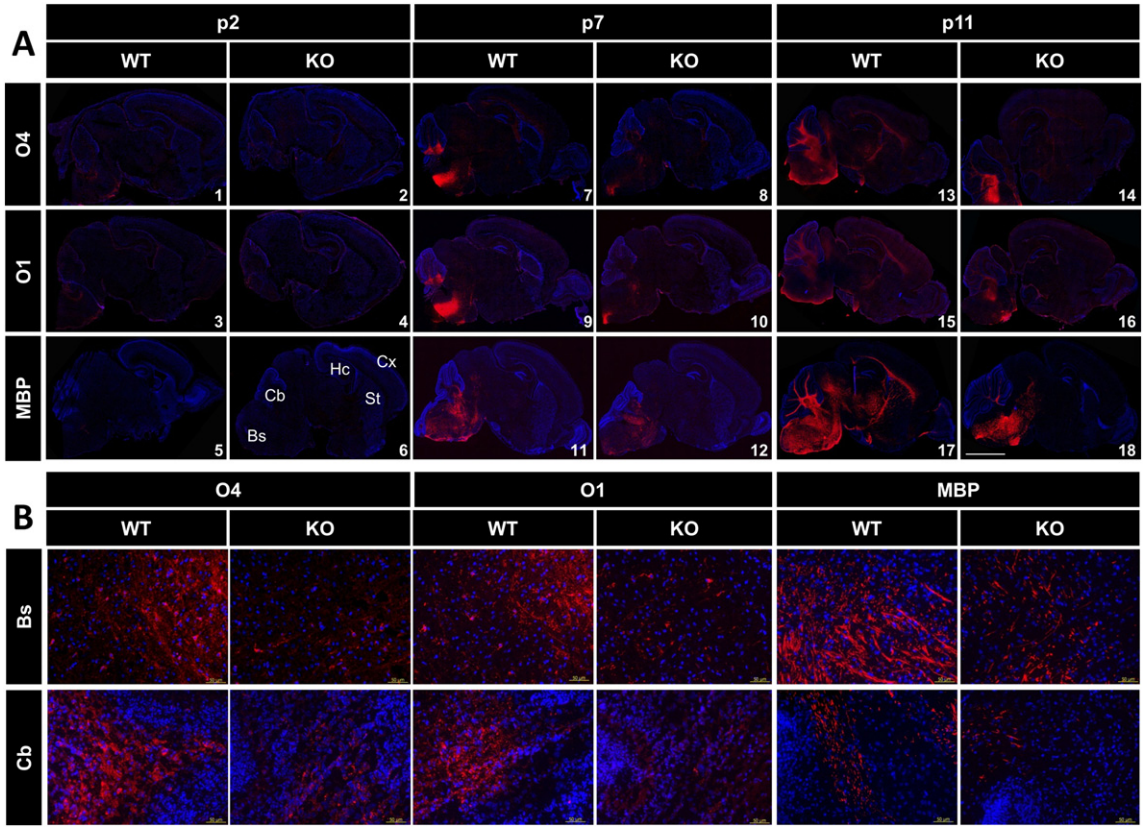

Fig. 9. Spatiotemporal differences in myelin and oligodendrocyte lineage marker expression during postnatal development in sialin-deficient mice. (A) Overview images (10× magnification) of mouse brain longitudinal sections from *Slc17a5*$^{+/+}$ (WT) and *Slc17a5*$^{-/-}$ (KO) mice after immunofluorescence staining for different markers of oligodendrocyte progenitors (O4,O1) and mature myelinating oligodendrocytes (MBP) at postnatal stages p2, p7 and p11. Images represent planes corresponding to Paxinos and Watson (1986) specified levels varying from lateral level 0.9 mm up to lateral level 1.90 mm. Background morphology is indicated in panel 6; (B) representative high magnification images of O4, O1 & MBP immunofluorescence labeling at age p7. Red: O4-, O1- and MBP-labeling respectively. Blue: Hoechst nuclear counter stain. Scale bars: 50 μm; abbreviations: Bs: brainstem, Cb: cerebellum, Cx: cortex, Hc: hippocampus, St: striatum. (For interpretation of the references to color in this figure legend, the reader is referred to the web version of this article.)

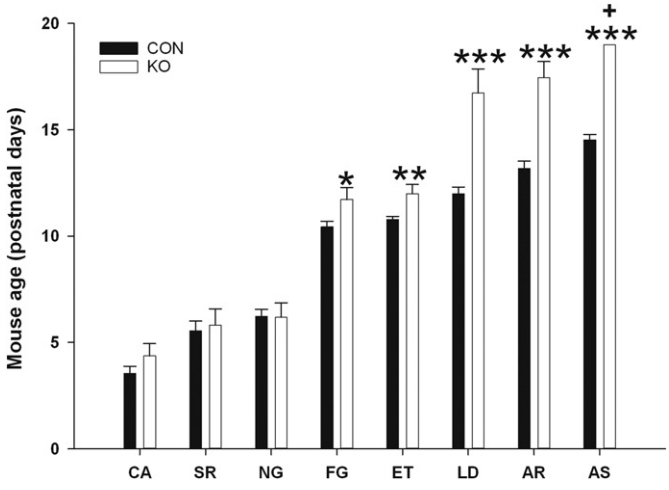

Fig. 10. Progressive delay of reaching developmental milestones in sialin-deficient mice. Earliest neurobehavioral milestones (CA, SR, NG) are achieved at similar time points by *Slc17a5*$^{-/-}$ mice (KO, white bars) in comparison to heterozygous and wildtype littermates (grouped together as controls (CON), black bars). However they show a progressive delay in reaching later milestones, with significantly retarded achievements for FG and ET and severe delays for LD, AR and AS. Data are presented as mean + SEM. Note: plus-sign indicates that the milestone behavior AS was not exhibited by any of the *Slc17a5*$^{-/-}$ mice during the observed period. Asterisks indicate significance of difference in comparison with control littermates (*t*-test; $^{*}p < 0.05$, $^{**}p < 0.01$, $^{***}p < 0.001$). Abbreviations: CA, cliff aversion; SR, surface righting; NG, negative geotaxis; FG, forelimb grasping; ET, ear twitch; LD, locomotion development; AR, air righting; AS, auditory startle.

in a mouse model of Canavan disease as well (Carpinelli et al., 2014; von Jonquieres et al., 2014).

The present report links sialin deficiency to impaired OL lineage development, and demonstrated that the resulting leukoencephalopathy causes a distinct pattern of neurodevelopmental dysfunctions. In general, sialin deficiency clearly impairs the complex mechanisms of brain myelination. Steps involved in the generation of oligodendrocytes and myelin correlate to events of remyelination after myelin damage. Studies in sialin knock-out mice could therefore also contribute to pathophysiological and therapeutic research about more common myelination disorders.

4. Materials & methods

4.1. Slc17a5 knockout mice

Slc17a5 knockout mice were developed in collaboration with Lexicon Genetics Inc. and presented in 2005 (Moechars et al., 2005). Animals were maintained in an SPF facility that meets all Belgian and European requirements for animal care. Mice were group-housed in a climate-controlled animal colony with a 12 h dark-light cycle (light on 7:00 EST) with free access to food and water, except during behavioral testing. Adequate measures were taken to minimize pain or discomfort. All experiments were carried out in accordance with the European Communities Council Directives (86/609/EEC) and were approved by the local ethical committee.

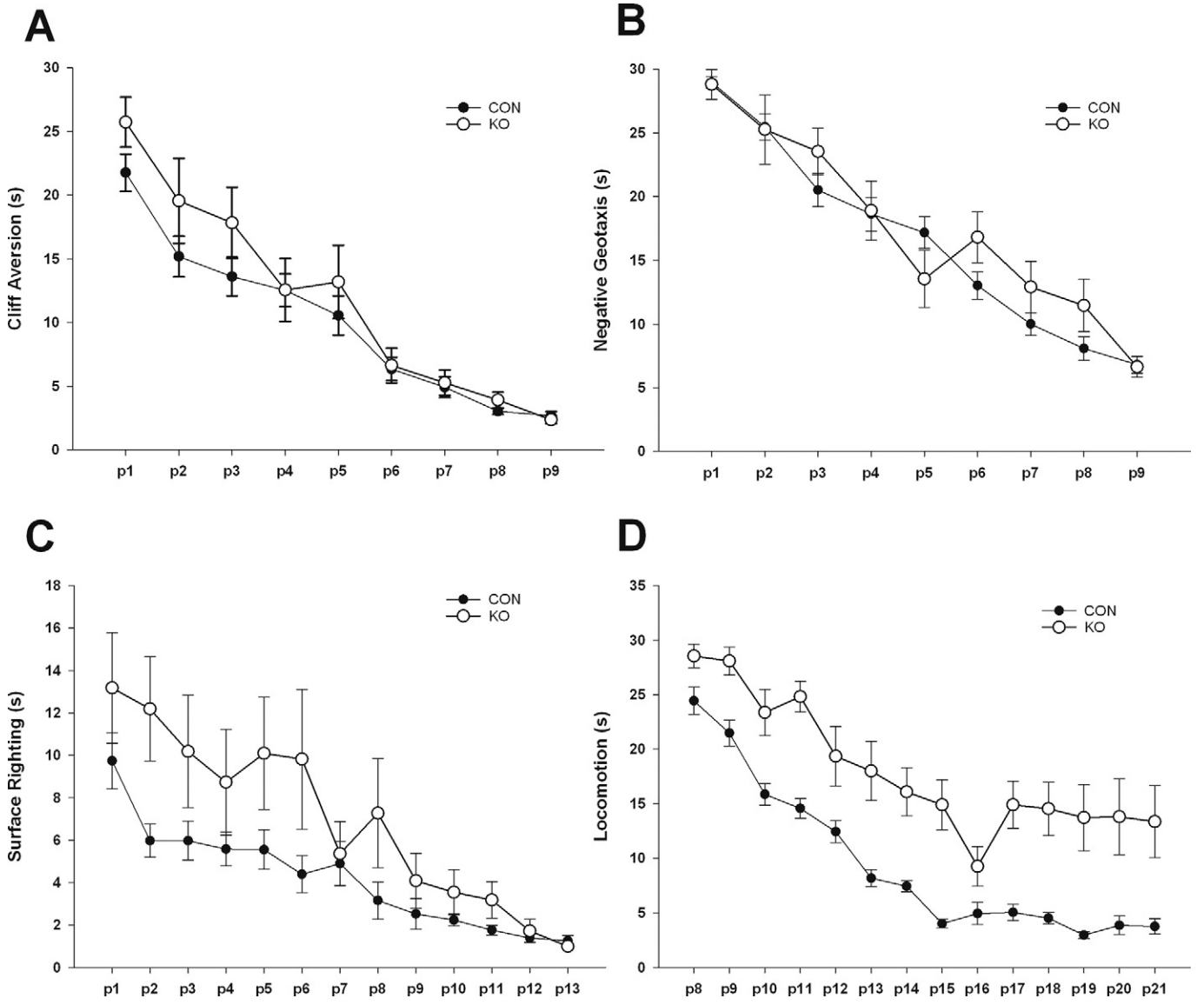

Fig. 11. Decreased performance of milestone behaviors in sialin-deficient mice. *Slc17a5*−/− mice (KO, white dots) show similar performance for milestone behaviors of cliff aversion and negative geotaxis in comparison to control littermates (CON, black dots). These mice showed reduced performance for surface righting however (main effect of genotype $p < 0.05$). They also showed increased exit latencies in the locomotion test, which were less pronounced during p8–9 and p16 (main effect of genotype $p < 0.001$, day × genotype interaction $p < 0.05$). Data are presented as mean + SEM.

4.2. Fibroblast isolation and free sialic acid measurement

Primary mouse embryonic fibroblast (MEF) cultures were established by standard procedures from individual embryonic day 13.5 (E13.5) embryos derived from heterozygous matings of *Slc17a5*$^{+/-}$ mice. Permanent *Slc17a5*$^{+/+}$, *Slc17a5*$^{+/-}$ and *Slc17a5*$^{-/-}$ cell lines were established from transformed clones arising spontaneously after repeated passage in culture (Todaro et al., 1963). MEFs were cultured in DMEM high glucose with L-glutamine, 10% FBS and penicillin/streptomycin. When confluent, cells were cryopreserved before sialic acid determination according to a modified thiobarbituric acid test (Mancini et al., 1991). Free sialic acid values from *Slc17a5*$^{+/+}$, *Slc17a5*$^{+/-}$ and *Slc17a5*$^{-/-}$ MEFs are compared to the diagnostic values of all clinical variants of SASD patients (infantile sialic acid storage disease (ISSD), intermediate SASD and Salla disease).

4.3. Biochemistry

In order to evaluate a defect of sialin function in *Slc17a5*$^{-/-}$ mice, the proton driven uptake of a sialin-substrate was evaluated using rat liver lysosomal vesicles (RLV) as a reference. Mouse livers were freshly dissected from 18 days old mice, either six *Slc17a5*$^{-/-}$, six *Slc17a5*$^{+/-}$, or six *Slc17a5*$^{+/+}$ mice, after overnight fasting. About 1.5 to 3 g wet weight livers were obtained from each mouse group. Lysosomal membrane vesicles were prepared using a differential centrifugation method as described (Mancini et al., 1989). Functional transport assays with lysosomal membrane vesicles were performed as described for rat livers with some adaptations as described for human lysosomal membrane vesicles, using tritiated glucuronic acid as a substrate (Mancini et al., 1991).

4.4. Micro-array analysis

Total brain RNA was isolated from newborn (p0) as well as 10 (p10) and 18 days (p18) old pups derived from heterozygous breeding pairs using the RNeasy kit (Qiagen, Venlo, Netherlands) combined with DNAse treatment. One microgram of extracted total RNA was biotin labeled and hybridized with the Mouse Genome 430 version 2.0 GeneChip array (Affymetrix, Orbassano, Italy). All data were processed by using the statistical computing R-program (R version 2.4.0) (R Development Core Team, URL www.R-project.org, 2006) and Bioconductor

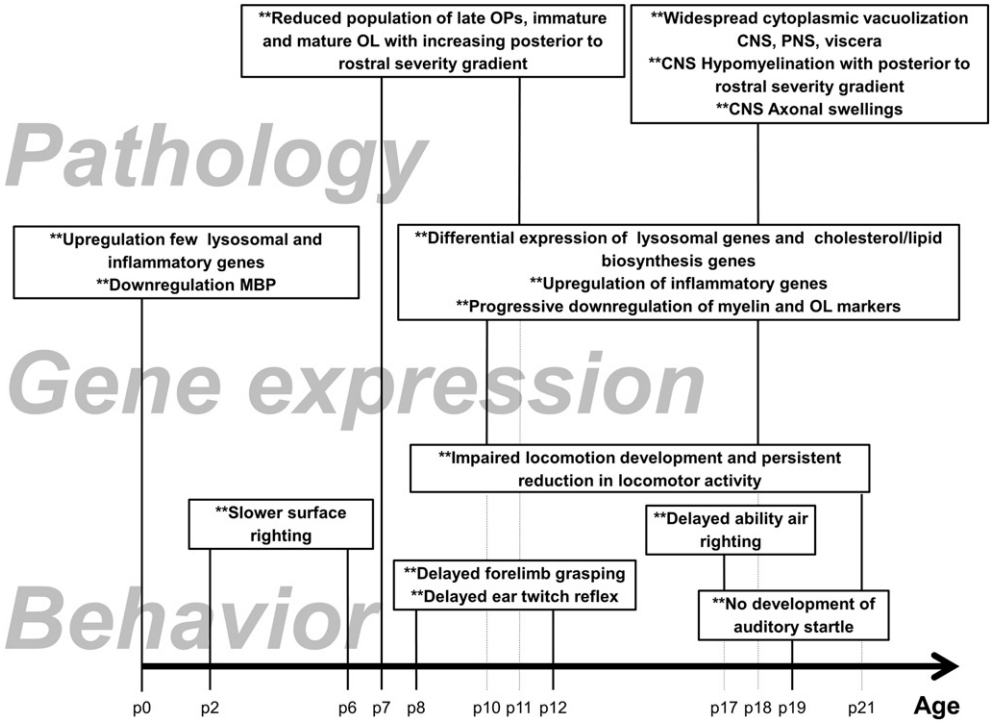

Fig. 12. Overview of age-dependent pathological, genetic and behavioral alterations in sialin-deficient mice characterized during the present study.

tools (Gentleman et al., 2004). Gene expressions were computed using the FARMS algorithm (Hochreiter et al., 2006). Grouping of the individual probes into gene-specific probe sets was performed based on the Entrez Gene using the metadata package mm430mmentrezg (version 8). All analysis of the microarray data were done at three levels: spectral map analysis (Wouters et al., 2003), significance analysis of microarray (SAM, at FDR < 0.005) (Tusher et al., 2001) and analysis of affected processes.

4.5. Tissue processing for histology

Five Homozygous *Slc17a5*$^{-/-}$ and five *Slc17a5*$^{+/+}$ mice were sacrificed by cervical dislocation and decapitation at p18. Brain tissue and spinal cord were embedded in paraffin or cryopreservation in OCT by freezing at −40 °C. To study the OL lineage, brain tissue of *Slc17a5*$^{-/-}$ and *Slc17a5*$^{+/+}$ mice at p2, p7 and p11 was processed in the same way. Paraffin embedded material was sectioned at 6 μm whereas cryopreserved samples were sectioned at 10 μm. Ischiadic nerves were processed by plastic embedding.

4.6. Histology

Routine morphological evaluation of all tissue sections was performed on hematoxylin phloxin saffrane (HPS) stained sections and Nissl stained sections for brain specific questions. Toluidine Blue staining was used to investigate peripheral nerve morphology.

4.7. Immunohistochemistry

LAMP-1 (lysosomal associated membrane protein, isoform 1) (Abcam, Cambridge, UK) (1/500) and GFAP (Dako Cytomation, 1/100) staining was performed after heat-induced epitope retrieval and visualized by Envision + System-HRP Labeled Polymer (Dako, Denmark), followed by DAB.

4.8. Immunofluorescence techniques

All immunofluorescence stains on deparaffinised sections required an enzymatic pre-treatment of trypsin followed by heat mediated microwave antigen retrieval using EDTA. Immunohistochemistry on 10 μm thick cryosections required 4% paraformaldehyde fixation prior to incubation with the primary antibodies. Prior to incubation with mouse monoclonal antibodies, blocking stages were performed using 10% normal goat serum (Dako, Denmark) with subsequent endogenous mouse IgG blocking (Goat-anti-Mouse F'ab fragments, Jackson Immunoresearch Laboratories, Inc., PA, USA). Mouse monoclonal antibodies used are: anti-MBP (SMI-94, Abcam Ltd., Cambridge, UK) (1/1000), anti-O1 and -O4 (Chemicon Int., CA USA) (1/100) and anti-neurofilament proteins of 70- and 200-kDa (Euro-Diagnostica bv, Netherlands) (1/100). These monoclonal antibodies were visualized using Cy3 conjugated goat anti-mouse IgG (Jackson Immunoresearch Laboratories, Inc., PA, USA) (1/500), Alexa555 conjugated goat anti-mouse IgM (Invitrogen Corporate, Molecular Probes, California, USA) (1/500) or Alexa488 conjugated goat anti-mouse IgG (Invitrogen Corporate, Molecular Probes, California, USA) (1/100) depending on the application. Rabbit polyclonal antibodies used are anti-GFAP (Dako Cytomation) (1/100) and anti-MBP (Abcam Ltd., Cambridge, UK) (1/100). These are visualized by Cy3 conjugated goat anti-rabbit IgG (Jackson Immunoresearch Laboratories, Inc., PA, USA) (1/500) or Alexa488 conjugated goat anti-rabbit IgG (Invitrogen Corporate, Molecular Probes, California, USA) (1/100) depending on the application. All sections were counterstained with Hoechst (Invitrogen Corporate, Molecular Probes, California, USA) (1/500).

4.9. Imaging and analysis

Imaging was performed on Axioplan-2 Imaging microscope (Carl Zeiss, Germany) equipped with a high resolution Axiocam camera and the Multidimensional and Mosaics modules of the imaging software Axiovision Release 4.6. Quantitative analysis of the number of cortical neuronal and non-neuronal cells and of cerebellar Purkinje cells was

performed in 10 fields at a 63× magnification in transversal sections of 5 *Slc17a5*$^{-/-}$ and *Slc17a5*$^{+/+}$ mouse brains at P18. The 10 regions analyzed were randomly chosen throughout the entire cortex and Purkinje cell layer. One region corresponds to 0.096 mm^2 using a 63× objective and eyepiece with field number 22. Results were analyzed by a non-parametrical Wilcoxon Krüskal-Wallis test.

4.10. Neurobehavioral development

Developmental milestones were daily evaluated in neonatal mice of all genotypes (p1–p21). No obvious differences were observed between heterozygous and wildtype mice, hence they were compared as one control group (n = 38) to performance of sialin knockout mice (n = 11). The developmental test battery (adapted from (Hill et al., 2008)) involved assessment of milestone achievement and speed of execution of milestone behaviors. Specifically, the following behaviors were examined during the relevant period of age: surface righting (time for a pup to turn over after being held on its back; max 30 s – milestone criterion 1 s); negative geotaxis (time for a pup to turn after being placed head-down on a 45° slope; max 30 s – milestone criterion <10 s); cliff aversion (time for a pup, placed at the edge of a plastic box, to turn away from the edge; max 30 s – milestone criterion <10 s); forelimb grasping (ability of a pup to grip a thin bar with its forepaws; milestone criterion 1 s); locomotion development (time for a pup to exit a 13-cm diameter circle; max 30 s – milestone criterion <10 s); air righting (ability of a pup, after being held upside down and released at ~11 cm height, to turn and land on all paws). Sensory developmental markers were also evaluated: auditory startle (appearance of a startle response to a handclap at ~10 cm); ear twitch (appearance of ear twitching after tactile stimulation with a cotton swab tip). If the milestone behavior was not exhibited during the observed time period, milestone achievement was quantified as 'last day of testing + 1'. Data were analyzed using *t*-tests (for milestone achievement data) and repeated-measures ANOVA (for performance data).

4.11. Open field test

A panel of eight *Slc17a5*$^{+/+}$, eight *Slc17a5*$^{+/-}$ and five *Slc17a5*$^{-/-}$, aged between six and seven weeks were subjected to the OFT, which was performed during the light phase of a normal light/dark cycle. A large arena (40 cm × 40 cm) with infrared beams at three different levels was used to record rearing and locomotor activity. The animal was placed in the center and its activity was measured for 20 min. Data from this test were analyzed in five, 4-minute intervals. The total distance traveled (cm) and vertical movement number (rearing) were recorded. Data were analyzed using a *t*-test.

Funding

This work was supported by EU grant (EU/ALPHA-MAN 261331), federal science fund (FWO) grant G.0587.14 and a personal grant to SS from the MM Delacroix Foundation.

Conflict of interest statement

The authors declare that there is no conflict of interest.

References

Altman, J., Sudarshan, K., 1975. Postnatal development of locomotion in the laboratory rat. Anim. Behav. 23, 896–920.
Back, S.A., Han, B.H., Luo, N.L., Chricton, C.A., Xanthoudakis, S., Tam, J., Arvin, K.L., Holtzman, D.M., 2002. Selective vulnerability of late oligodendrocyte progenitors to hypoxia-ischemia. J. Neurosci. 22, 455–463.
Barateiro, A., Fernandes, A., 2014. Temporal oligodendrocyte lineage progression: in vitro models of proliferation, differentiation and myelination. Biochim. Biophys. Acta 1843, 1917–1929.
Baumann, N., Pham-Dinh, D., 2001. Biology of oligodendrocyte and myelin in the mammalian central nervous system. Physiol. Rev. 81, 871–927.
Bercury, K.K., Macklin, W.B., 2015. Dynamics and mechanisms of CNS myelination. Dev. Cell 32, 447–458.
Biancheri, R., Verbeek, E., Rossi, A., Gaggero, R., Roccatagliata, L., Gatti, R., van Diggelen, O., Verheijen, F.W., Mancini, G.M., 2002. An Italian severe Salla disease variant associated with a SLC17A5 mutation earlier described in infantile sialic acid storage disease. Clin. Genet. 61, 443–447.
Carpinelli, M.R., Voss, A.K., Manning, M.G., Perera, A.A., Cooray, A.A., Kile, B.T., Burt, R.A., 2014. A new mouse model of Canavan leukodystrophy displays hearing impairment due to central nervous system dysmyelination. Dis. Model. Mech. 7, 649–657.
Craig, A., Ling Luo, N., Beardsley, D.J., Wingate-Pearse, N., Walker, D.W., Hohimer, A.R., Back, S.A., 2003. Quantitative analysis of perinatal rodent oligodendrocyte lineage progression and its correlation with human. Exp. Neurol. 181, 231–240.
Deng, W., 2010. Neurobiology of injury to the developing brain. Nat. Rev. Neurol. 6, 328–336.
El Waly, B., Macchi, M., Cayre, M., Durbec, P., 2014. Oligodendrogenesis in the normal and pathological central nervous system. Front. Neurosci. 8, 145.
Emery, B., Agalliu, D., Cahoy, J.D., Watkins, T.A., Dugas, J.C., Mulinyawe, S.B., Ibrahim, A., Ligon, K.L., Rowitch, D.H., Barres, B.A., 2009. Myelin gene regulatory factor is a critical transcriptional regulator required for CNS myelination. Cell 138, 172–185.
Falahati, S., Breu, M., Waickman, A.T., Phillips, A.W., Arauz, E.J., Snyder, S., Porambo, M., Goeral, K., Comi, A.M., Wilson, M.A., et al., 2013. Ischemia-induced neuroinflammation is associated with disrupted development of oligodendrocyte progenitors in a model of periventricular leukomalacia. Dev. Neurosci. 35, 182–196.
Fletcher, J.L., Kondagari, G.S., Wright, A.L., Thomson, P.C., Williamson, P., Taylor, R.M., 1812. Myelin genes are downregulated in canine fucosidosis. Biochim. Biophys. Acta 1418–1426.
Gentleman, R.C., Carey, V.J., Bates, D.M., Bolstad, B., Dettling, M., Dudoit, S., Ellis, B., Gautier, L., Ge, Y., Gentry, J., et al., 2004. Bioconductor: open software development for computational biology and bioinformatics. Genome Biol. 5, R80.
Haataja, L., Parkkola, R., Sonninen, P., Vanhanen, S.L., Schleutker, J., Aarimaa, T., Turpeinen, U., Renlund, M., Aula, P., 1994. Phenotypic variation and magnetic resonance imaging (MRI) in Salla disease, a free sialic acid storage disorder. Neuropediatrics 25, 238–244.
Havelaar, A.C., Mancini, G.M., Beerens, C.E., Souren, R.M., Verheijen, F.W., 1998. Purification of the lysosomal sialic acid transporter. Functional characteristics of a monocarboxylate transporter. J. Biol. Chem. 273, 34568–34574.
Hill, J.M., Lim, M.A., Stone, M.M., 2008. Developmental milestones in the newborn mouse. In: Gozes, I. (Ed.), Neuropeptide Techniques. Humana Press Inc., Totowa, NJ, pp. 131–149.
Hochreiter, S., Clevert, D.A., Obermayer, K., 2006. A new summarization method for Affymetrix probe level data. Bioinformatics 22, 943–949.
Kaartinen, V., Mononen, I., Voncken, J.W., Noronkoski, T., Gonzalez-Gomez, I., Heisterkamp, N., Groffen, J., 1996. A mouse model for the human lysosomal disease aspartylglycosaminuria. Nat. Med. 2, 1375–1378.
Kessaris, N., Fogarty, M., Iannarelli, P., Grist, M., Wegner, M., Richardson, W.D., 2006. Competing waves of oligodendrocytes in the forebrain and postnatal elimination of an embryonic lineage. Nat. Neurosci. 9, 173–179.
Lemyre, E., Russo, P., Melancon, S.B., Gagne, R., Potier, M., Lambert, M., 1999. Clinical spectrum of infantile free sialic acid storage disease. Am. J. Med. Genet. 82, 385–391.
Lovell, K.L., Jones, M.Z., 1985. Axonal and myelin lesions in beta-mannosidosis: ultrastructural characteristics. Acta Neuropathol. 65, 293–299.
Low, H.P., Greco, B., Tanahashi, Y., Gallant, J., Jones, S.N., Billings-Gagliardi, S., Recht, L.D., Schwartz, W.J., 2009. Embryonic stem cell rescue of tremor and ataxia in myelin-deficient shiverer mice. J. Neurol. Sci. 276, 133–137.
Malone, M.J., 1976. The cerebral lipidoses. Pediatr. Clin. N. Am. 23, 303–326.
Mancini, G.M., de Jonge, H.R., Galjaard, H., Verheijen, F.W., 1989. Characterization of a proton-driven carrier for sialic acid in the lysosomal membrane. Evidence for a group-specific transport system for acidic monosaccharides. J. Biol. Chem. 264, 15247–15254.
Mancini, G.M., Beerens, C.E., Aula, P.P., Verheijen, F.W., 1991. Sialic acid storage diseases. A multiple lysosomal transport defect for acidic monosaccharides. J. Clin. Invest. 87, 1329–1335.
Miller, R.H., 2002. Regulation of oligodendrocyte development in the vertebrate CNS. Prog. Neurobiol. 67, 451–467.
Miller, R.H., 2005. Dorsally derived oligodendrocytes come of age. Neuron 45, 1–3.
Moechars, D., Van Acker, N., Cryns, K., Andries, L., Mancini, G., Verheijen, F., 2005. Sialin-deficient mice: a novel animal model for infantile free sialic acid storage disease (ISSD). Society for Neuroscience 35th Annual Meeting, Washington, USA.
Morse, R.P., Kleta, R., Alroy, J., Gahl, W.A., 2005. Novel form of intermediate salla disease: clinical and neuroimaging features. J. Child Neurol. 20, 814–816.
Parazzini, C., Arena, S., Marchetti, L., Menni, F., Filocamo, M., Verheijen, F.W., Mancini, G.M., Triulzi, F., Parini, R., 2003. Infantile sialic acid storage disease: serial ultrasound and magnetic resonance imaging features. AJNR Am. J. Neuroradiol. 24, 398–400.
Paxinos, G., Watson, Ch, 1986. The Rat Brain in Stereotactic Coordinates. Second Edition. Academic Press, Australia.
Prolo, L.M., Vogel, H., Reimer, R.J., 2009. The lysosomal sialic acid transporter sialin is required for normal CNS myelination. J. Neurosci. 29, 15355–15365.
Regis, S., Biancheri, R., Bertini, E., Burlina, A., Lualdi, S., Bianco, M.G., Devescovi, R., Rossi, A., Uziel, G., Filocamo, M., 2008. Genotype-phenotype correlation in five Pelizaeus-Merzbacher disease patients with PLP1 gene duplications. Clin. Genet. 73, 279–287.
Ruivo, R., Sharifi, A., Boubekeur, S., Morin, P., Anne, C., Debacker, C., Graziano, J.C., Sagne, C., Gasnier, B., 2008. Molecular pathogenesis of sialic acid storage diseases: insight gained from four missense mutations and a putative polymorphism of human sialin. Biol. Cell. 100, 551–559.

Sonninen, P., Autti, T., Varho, T., Hamalainen, M., Raininko, R., 1999. Brain involvement in Salla disease. AJNR Am. J. Neuroradiol. 20, 433–443.
Steenweg, M.E., Vanderver, A., Blaser, S., Bizzi, A., de Koning, T.J., Mancini, G.M.S., van Wieringen, W.N., Barkhof, F., Wolf, N.I., van der Knaap, M.S., 2010. Magnetic resonance imaging pattern recognition in hypomyelinating disorders. Brain 133, 2971–2982.
Suzuki, K., 2003. Globoid cell leukodystrophy (Krabbe's disease): update. J. Child Neurol. 18, 595–603.
Todaro, G.J., Wolman, S.R., Green, H., 1963. Rapid transformation of human fibroblasts with low growth potential into established cell lines by Sv40. J. Cell. Physiol. 62, 257–265.
Tusher, V.G., Tibshirani, R., Chu, G., 2001. Significance analysis of microarrays applied to the ionizing radiation response. Proc. Natl. Acad. Sci. U. S. A. 98, 5116–5121.
van der Lei, H.D., van Berkel, C.G., van Wieringen, W.N., Brenner, C., Feigenbaum, A., Mercimek-Mahmutoglu, S., Philippart, M., Tatli, B., Wassmer, E., Scheper, G.C., et al., 2010. Genotype-phenotype correlation in vanishing white matter disease. Neurology 75, 1555–1559.
Varho, T., Jaaskelainen, S., Tolonen, U., Sonninen, P., Vainionpaa, L., Aula, P., Sillanpaa, M., 2000. Central and peripheral nervous system dysfunction in the clinical variation of Salla disease. Neurology 55, 99–104.
Verheijen, F.W., Verbeek, E., Aula, N., Beerens, C.E., Havelaar, A.C., Joosse, M., Peltonen, L., Aula, P., Galjaard, H., van der Spek, P.J., et al., 1999. A new gene, encoding an anion transporter, is mutated in sialic acid storage diseases. Nat. Genet. 23, 462–465.
von Jonquieres, G., Froud, K.E., Klugmann, C.B., Wong, A.C., Housley, G.D., Klugmann, M., 2014. Loss of central auditory processing in a mouse model of Canavan disease. PLoS One 9, e97374.
Walkley, S.U., Sikora, J., Micsenyi, M., Davidson, C., Dobrenis, K., 2010. Lysosomal compromise and brain dysfunction: examining the role of neuroaxonal dystrophy. Biochem. Soc. Trans. 38, 1436–1441.
Warrington, A.E., Barbarese, E., Pfeiffer, S.E., 1993. Differential myelinogenic capacity of specific developmental stages of the oligodendrocyte lineage upon transplantation into hypomyelinating hosts. J. Neurosci. Res. 34, 1–13.
Wouters, L., Gohlmann, H.W., Bijnens, L., Kass, S.U., Molenberghs, G., Lewi, P.J., 2003. Graphical exploration of gene expression data: a comparative study of three multivariate methods. Biometrics 59, 1131–1139.
Wreden, C.C., Wlizla, M., Reimer, R.J., 2005. Varied mechanisms underlie the free sialic acid storage disorders. J. Biol. Chem. 280, 1408–1416.
Yan, X., Lukas, J., Witt, M., Wree, A., Hubner, R., Frech, M., Kohling, R., Rolfs, A., Luo, J., 2011. Decreased expression of myelin gene regulatory factor in Niemann-Pick type C 1 mouse. Metab. Brain Dis. 26, 299–306.